Filtering Airborne Laser Scanning Data with Morphological Methods

Qi Chen, Peng Gong, Dennis Baldocchi, and Gengxin Xie

Abstract

Filtering methods based on morphological operations have been developed in some previous studies. The biggest challenge for these methods is how to keep the terrain features unchanged while using large window sizes for the morphological opening. Zhang et al. (2003) tried to achieve this goal, but their method required the assumption that the slope is constant. This paper presents a new method to achieve this goal without such restrictions, and methods for filling missing data and removing outliers are proposed. The experimental test results using the ISPRS Commission III/WG3 dataset show that this method performs well for most sites, except those with missing data due to the lack of overlap between swaths. This method also shows encouraging results for laser data with low pulse density.

Introduction

Airborne laser scanning (ALS) is gaining popularity in various environmental applications, ranging from DEM mapping, transportation, and urban studies to forest management, hydrology, and ecology (Flood and Gutelius, 1997). Compared with digital photogrammetry (Gong *et al.*, 2000; Sheng *et al.*, 2001; Gong *et al.*, 2002) and radar interferometry (Hoekman and Varekamp, 1998), laser altimetry has the advantage of recording the elevation of earth surface directly. Nevertheless, there is a great need for efficient data processing methods (Axelsson, 1999). In particular, filtering, the abstraction of bare earth from ALS points, is a crucial procedure for ALS data processing (Sithole and Vosselman, 2004). It, with quality control, generally consumes an estimated 60 to 80 percent of processing time (Flood, 2001). However, the details of filtering algorithms were seldom reported due to the tendency of some commercial and academic practitioners to keep their work proprietary (Haugerud and Harding, 2001; Huising and Gomes-Pereira, 1998; Sithole and Vosselman, 2004).

Sithole and Vosselman (2004) divided current filtering algorithms into four categories including slope-based, block-minimum, surface-based, and clustering/segmentation methods, among which the surface-based method is widely used. The idea of surface-based methods is to create a surface with a corresponding buffer zone above it, and the buffer zone defines the region in 3D space where terrain points are expected to reside (Sithole and Vosselman, 2004). The key of this method is to create a surface approximating the bare earth. Depending on the means of creating the surface, surface-based filtering methods can be further divided into the following two subcategories:

1. Interpolation-based Methods: Kraus and Pfeifer (1998) proposed an algorithm to iteratively approximate the ground using weighted linear least squares interpolation. Since terrain points usually have negative residuals and non-terrain points have positive ones, a weight function was designed to assign high weight to the points with negative residuals. This algorithm was extended by incorporating the hierarchical approach (Pfeifer *et al.*, 2001), and it was found that the hierarchical interpolation can improve the filter result and speed up the computation. Lee and Younan (2003) improved Kraus and Pfeifer's method by replacing the least squares method with a normalized least squares method called adaptive line enhancement (ALE). The implementation of ALE required *a priori* knowledge of a number of parameters such as the delay factor and the adaptation parameter. In another study, iterative regression was also used by Brandtberg *et al.* (2003) to derive DEM in a forest area.
2. Morphological Methods: The idea of morphological methods is approximating the terrain surface using morphological operations such as opening. Compared with other methods, morphological methods are conceptually simple and can be easily implemented. When there are enough pulses reaching the ground, morphological opening with a small window size can effectively remove the surface objects and generate a surface approximating the ground. However, when there are not many pulses hitting the ground, such as the places where buildings are located, the window size for morphological opening has to be large to remove the objects. The problem of using a morphological opening with larger window sizes is that it will produce a surface with more protruded terrain features flattened. Therefore, how to keep the terrain features unchanged while using large window sizes for opening is the biggest challenge.

Qi Chen is with the Center for the Assessment and Monitoring of Forest and Environmental Resources CAMFER), University of California at Berkeley, Berkeley, CA 94720 (qch@nature.berkeley.edu).

Peng Gong is with the Center for the Assessment and Monitoring of Forest and Environmental Resources CAMFER), University of California at Berkeley, Berkeley, CA 94720 and also with the State Key Lab of Remote Sensing Science (jointly sponsored by Institute of Remote Sensing Applications, Chinese Academy of Sciences, and Beijing Normal University), Postal Box 9718, Beijing, P.R. China 100101 (gong@nature.berkeley.edu).

Dennis Baldocchi is with the Department of Environmental Science, Policy, and Management, University of California at Berkeley, Berkeley, CA 94720 (baldocchi@nature.berkeley.edu).

Gengxin Xie is with the School of Environmental Science & Engineering, Hunan University, Changsha, Hunan, 410082, China.

Photogrammetric Engineering & Remote Sensing
Vol. 73, No. 2, February 2007, pp. 000–000.

0099-1112/07/7302–0000/$3.00/0
© 2007 American Society for Photogrammetry and Remote Sensing

Some researchers have made efforts in trying to solve this problem. Kilian *et al.* (1996) used different window sizes into their data set starting from the smallest one; then, each point was assigned a weight related to the window size if it was classified as a ground point, and the terrain surface was estimated by using all points with assigned weights. Zhang *et al.* (2003) proposed a method to remove surface objects while preserving terrain using gradually increased window sizes. They compared the elevation difference between surfaces after morphological opening with successively increased window sizes. If the elevation difference of a point was less than a threshold, it was classified as a terrain point. The threshold was determined by the terrain slope. The major limitation of this method is that it assumed the slope over an area is constant, and the slope had to be chosen by iteratively comparing the filtered and unfiltered data. The assumption of a constant slope is not always realistic, especially for complex scenes. If the actual terrain slope is greater the predetermined slope, the points will be classified as non-terrain points. Correspondingly, the omission errors of identifying terrain points will increase.

The objective of this paper is to present a method that can remove non-ground objects and preserve terrain features during the morphological opening, even with large window sizes. Similar to Zhang *et al.* (2003)'s method, progressively increased window sizes are used for morphological operations. However, the method of this study doesn't require the assumption of a constant slope. The method is developed based on the fact that non-terrain objects such as buildings usually have abrupt elevation changes along their boundaries while the change of terrain elevation is gradual and continuous. Since this fact typically holds, this method is adaptive to local terrain and can readily work over rugged areas. To evaluate its performance, this method is compared with a benchmark study conducted by ISPRS Commission III/WG 3 (Sithole and Vosselman, 2004), which tested eight filtering algorithms over sites ranging from urban to rural areas with different complexity.

Methods

This section is organized as follows: (a) for completeness, some concepts of morphological operations are revisited first, and the remainder of this section introduces the steps of processing; (b) the first step of this method is to fill missing data since missing data exist in the dataset we used; (c) after missing data have been filled and a grid has been created, the objects on the ground can be removed by morphological opening with progressively increased windows sizes. Vegetated areas typically require smaller window sizes than built areas since laser pulses can penetrate canopy and reach the ground. In this step, how to determine the minimum window size in vegetated areas is discussed. After a morphological opening with the minimum window size, trees have been removed in the surface, with large objects such as buildings remaining; (d) a common issue in the data set is the existence of outliers, which are unrealistically higher or lower than their surrounding terrain. The higher outliers can be removed in the morphological opened surface, while the lower outliers cannot. Therefore, a method is developed to detect the lower outliers and fill the surface; (e) after the trees and outliers are removed, the next step is to remove large artificial objects such as buildings. An algorithm is designed to remove buildings using progressively increased window sizes and avoid cutting terrain features; and (f) finally, terrain points are extracted from the approximated surface and a DEM is generated.

Morphological Operations

Mathematical morphology stems from set theory and is widely used in image processing (Soille, 2003). The basic operations in mathematical morphology are erosion and dilation, which are performed over a neighborhood specified by a structural element. The erosion of a set X by a structural element B is denoted by:

$$[\varepsilon_B(X)](x) = \min\{x_B\} \tag{1}$$

where $[\varepsilon_B(X)](x)$ means the erosion of x in X with structural element B, and x_B means values within x's neighborhood specified by B. Conversely, the dilation of a set X by a structural element B is:

$$[\delta_B(X)](x) = \max\{x_B\}. \tag{2}$$

In the following methods, a circular or "disk" structural element is used since a circular structural element is more suitable for removing trees and preserving terrain.

Consider a one-dimensional laser point series evenly distributed (Figure 1a): erosion is to obtain the elevation of the lowest point within its neighborhood, and dilation is to obtain the elevation of the highest point within its neighborhood. Based on erosion and dilation, two other operations, opening and closing, can be derived. Opening means erosion followed by dilation while closing means dilation followed by erosion. A nice property of opening is that it can remove "outstanding" objects smaller than the specified neighborhood window size. For example, when the neighborhood of a point is defined to be its nearest three points, the tree B in Figure 1 will be removed (Figure 1b) and the elevation of each point will be updated with the value after morphological opening. The updated elevation can approximate the bare earth well, especially over flat areas. Comparing the original elevation with the opened elevation of each laser point, a laser point will be classified as a terrain point if the difference is less than a threshold, otherwise it will be an object point.

The importance of window sizes can be demonstrated in Figure 1. Whatever a window size is, the morphological opening will flatten any protruded terrain feature within the window size (see C in Figure 1b and 1c). When a larger window size is needed to remove large objects such as building A, more terrain will be flattened and cut off. This can be observed by comparing the terrain after opening around the location C in Figure 1b and 1c.

Rasterization and Filling Missing Data

Morphological operations are typically performed over a grid. Thus, the first step of this method is to record the elevation of the last return of each pulse into a grid. Because the minimum point spacing for the data used in this study is about 1 m, the grid size is set to be 1 m by 1 m. If there are several pulses falling in one cell, only the minimum elevation is recorded. This grid is denoted as $g_{\min}$ (Figure 2a). As in Zhang *et al.* (2003), the X and Y positions of the lowest pulse for each cell are also recorded. When the pulse spacing is greater than the 1 m, there are no values for some cells. For these cells, the general strategy is to iteratively fill them with the elevation of the nearest cell that has a value. However, problems occur when there are large areas of missing data. In the upper-left of the area shown in Figure 2 exist missing data caused by the water in the river since water is highly absorptive in the laser wavelength (1064 nm for the Optech instrument). There are trees alongside the river, leading to artifacts in the filled grid (Figure 2b).

Missing data could be typically identified due to three factors: (a) lack of overlap between laser swaths. (Usually, side overlap is required between laser swaths to guarantee

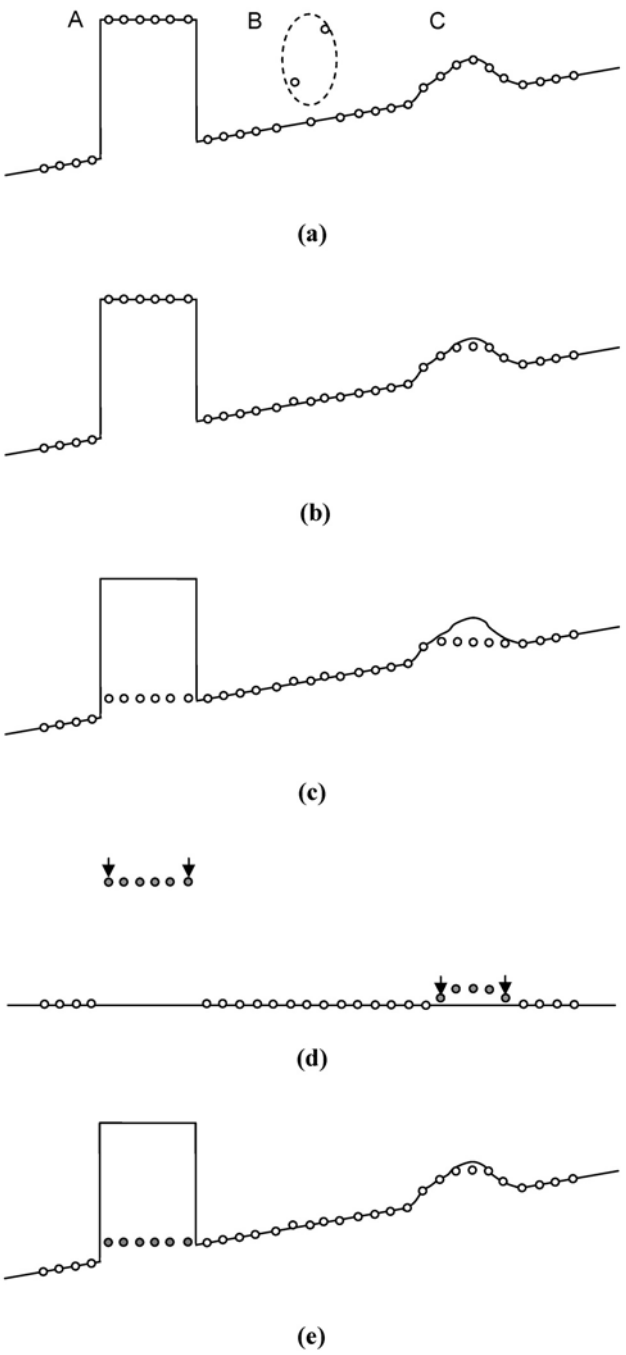

Figure 1. Example of one-dimensional laser points: (a) measured points, (b) points whose elevations are updated by opening with a neighborhood of 3 (*originalOpen*), (c) points whose elevations are updated by opening with a neighborhood of 7 (*newOpen*), (d) the point-wise difference between *originalOpen* and *newOpen*, and (c), and (e) the updated *originalOpen* after one iteration (the gray points are the updated points).

continuous data coverage, but data gaps can be produced due to the yaw, roll, and pitch of the airplane, (b) instrument malfunction, and (c) absorption of laser pulses by highly absorptive materials, typically water bodies. The first two problems can be avoided by well-planned operations. However, the missing data caused by absorptive materials have to be filled with some data processing techniques. Since water is the most typical material that causes large-area absorption, a technique for filling missing data is developed as follows specifically for water. Based on the fact that water usually has the lowest elevation among the adjacent areas, this technique is to find the areas of missing data and fill each area with the lowest elevation around it:

1. Locate the areas of having missing data. This is accomplished by (a) first creating a binary image where 1 stands for cells which have values and 0 for cells with no data (Figure 2c), and (b) then morphologically closing (dilation followed by erosion) this binary image with a "disk" structural element with radius r:

$$r = \left(\frac{1}{d}\right)^{0.5} \cdot \frac{1}{c} \tag{3}$$

   where d is the pulse density (number of pulses per square meter) and can be calculated from the raw data, c is the cell size in meter. $\left(\frac{1}{d}\right)^{0.5}$ is the average distance between pulses; therefore, $\left(\frac{1}{d}\right)^{0.5} \cdot \frac{1}{c}$ is the average cell number between two cells with values. After closing, the data gaps caused by sparse pulse density disappear and the large areas with missing data can be found (Figure 2d);

2. For each area, replace the values of $g_{\min}$ with the lowest elevation of cells within the boundary of each area. The boundary of each area is found by subtracting original area from the dilated area (Figure 2e). The structural element for dilating each area is a "disk" with radius of 1;
3. For the above modified $g_{\min}$, iteratively replace the cells of no values with the elevation of the nearest cell that has a value (Figure 2f). The difference between Figure 2b and Figure 2f shows the effects of missing data filling. This filled grid is denoted as $g_{f\min}$, each cell of which records the elevation of the nearest and lowest last return of laser pulses.

Filtering over Areas with Trees

In vegetated areas, the bare earth can be approximated by morphological opening $g_{f\min}$. As mentioned earlier, the window size used in morphological opening is critical. Consider laser point cloud in Figure 3a. They could hit on three completely different surfaces: (a) three trees above a flat terrain (Figure 3b), (b) three short vegetation (such as shrubs) over a slightly protruding terrain (Figure 3c), and (c) an over-rugged terrain (Figure 3d). Therefore, it is theoretically impossible to differentiate vegetation and terrain pulses and therefore choose window sizes only based on the spatial arrangement of laser points.

The morphologically-opened grid can approximate the bare earth better using the neighborhood window size containing at least one terrain return than larger window sizes. For example, if it is known that there is at least one terrain return every two laser pulses such as in Figure 3c, the neighborhood window size can be set to be its nearest three laser pulses (including itself). Therefore, ideally, the window size should be as small as possible but containing at least one terrain pulse. However, it is difficult to know whether there is at least one terrain pulse within a certain neighborhood window size. In practice, such a window size can be found by morphologically opening the filled grid $g_{f\min}$ with different window sizes and choosing the smallest one that can visually produce a smooth terrain. With such a method, it is possible to remove most, if not all, vegetation. This window size is denoted as $d_{\min}$. The opened grid of $g_{f\min}$ with $d_{\min}$ is called $g_{o(f\min)}$.

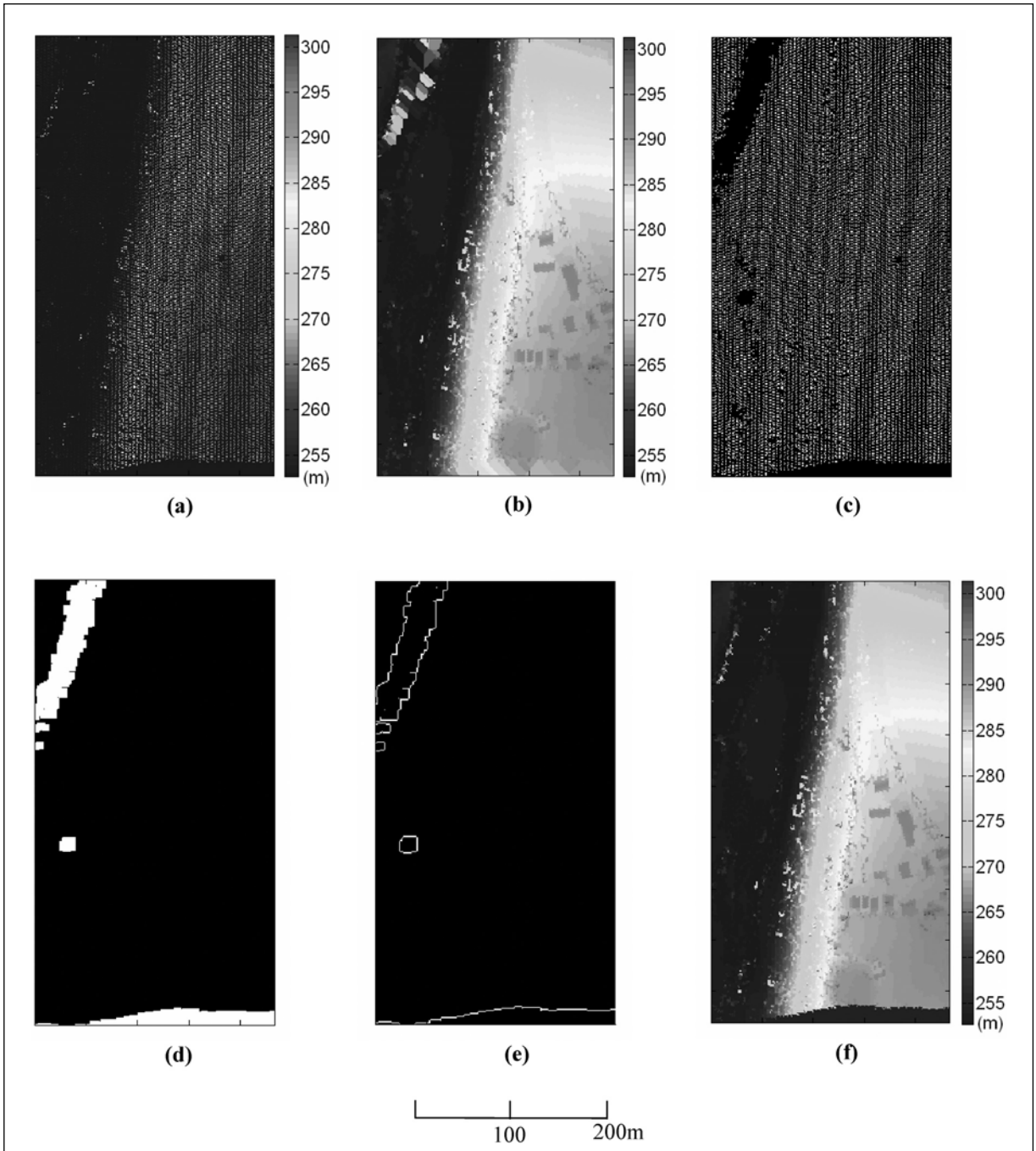

Figure 2. Rasterization and missing data filling: (a) $g_{\min}$, (b) filled raster with the nearest elevation before filling missing data, (c) binary grid indicating whether there are pulses within it, (d) the areas of missing data, (e) the boundary of each area in (d), and (f) filled raster with the nearest elevation after filling missing data. A color version of this figure is available at the ASPRS website: **www.asprs.org.**

Low Outliers Detecting and Filling

There are two kinds of outliers in the datasets of this study: high outliers and low outliers. Commonly, high outliers emerge from laser returns from birds, aircrafts, etc., and low outliers come from pulses that are reflected for several times or malfunction of a laser rangefinder (Sithole and Vosselman, 2004). High outliers can be removed by morphological opening. Thus, there are usually no high outliers in the opened grid $g_{o(f\,\min)}$. However, low outliers still exist (Figure 4a). Low outliers are assumed to be: (a) h meters lower than its surrounding cells, and (b) scattered. Based on these, low outliers are detected and filled as follows:

1. Compute the extended-minima transform of $g_{o(f\,\min)}$, denoted as $\mathrm{EMIN_h}(g_{o(f\,\min)})$. $\mathrm{EMIN_h}(g_{o(f\,\min)})$ is the regional minima of the h-minima transform of $g_{o(f\,\min)}$. The h-minima transformation of the $g_{o(f\,\min)}$ is to perform the reconstruction by erosion of $g_{o(f\,\min)}$ from $g_{o(f\,\min)} + h$:

$$g_{o(fmin),hmin} = R^{\varepsilon}_{g_{o(f\,min)}}(g_{o(f\,min)} + h) \tag{4}$$

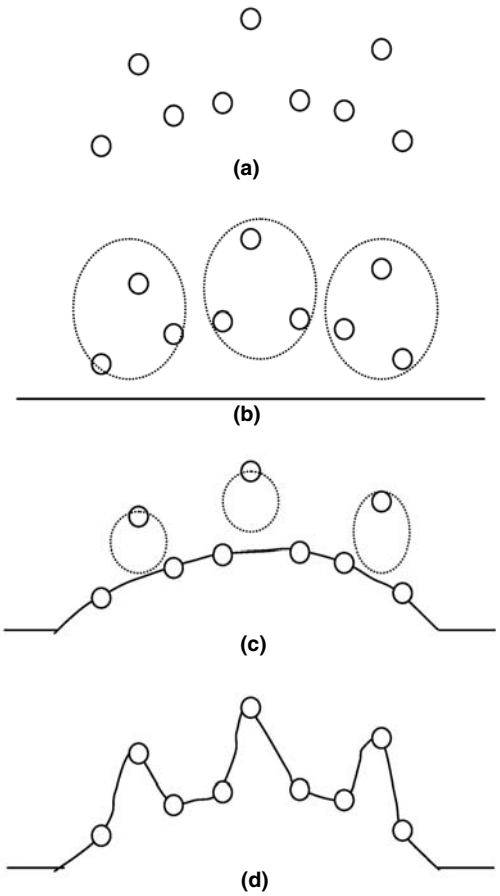

Figure 3. (a) arbitrary point cloud, which could hit (b) on three trees (indicated by dashed line), (c) on vegetation and terrain, and (d) on terrain only.

where $g_{o(f\,\min),h\,\min}$ is the h-minima transformation of $g_{o(f\,\min)}$ (Soille, 2003). The regional minima of $g_{o(f\,\min),h\,\min}$, EMIN_h ($g_{o(f\,\min)}$), was marked as treetops. An h-minima transform can fill up all regional minima the depths of which are less than h meters (Figure 4b). Note that the regional minima of $g_{o(f\,\min),h\,\min}$ include not only the minima caused by the outliers, but also the local minima of terrain (Figure 4c).

2. Select the regional minima of $\mathrm{EMIN}_h(g_{o(f\,\min)})$, the area of which are smaller than threshold a. Since outliers are scattered, only the regional minima smaller than a are classified as outlier areas.
3. Fill the cells of each outlier area using a similar procedure for filling missing data. That is, to find their boundary of each outlier area and fill cells of the area with the minimum elevation of their boundary cells (Figure 4d). The $g_{o(f\,\min)}$ with outliers removed and filled is denoted as $\tilde{g}_{o(f\,min)}$.

The choices of h and a are data-dependent and should be set by trial and error. The values of h and a are 3 m and 100 m^2, respectively for the dataset tested in this study.

Filtering Over Areas with Buildings

Assume trees have been removed in $\tilde{g}_{o(f\,min)}$. However, the window size d_{min} is usually not large enough to remove large objects such as buildings. Consider the one-dimensional example in Figure 1. When the window size is as small as three neighboring points, the building is kept intact although the tree has been removed (Figure 1b). As mentioned in the Morphological Operations section, when the window size increases to seven neighboring points, the building can be removed (see building A in Figure 1c); however, more protruded terrain will be cut off (see the location C in Figure 1c). The following method is used to determine whether the cut points are from buildings or terrain. Suppose there are points that are opened with a small window size called *orginalOpen* (Figure 1b). Now open these points with a larger window size and create new points called *newOpen* (Figure 1c). The cut points can be easily found by calculating the elevation differences between *newOpen* and *originalOpen*. For simplicity, assume the points with difference greater than zero are cut points (the gray points in Figure 1d). If considering the neighboring cut points as a group, it can be found that the group from building A has abrupt elevation changes along its edges, while the group from terrain C has little changes along its edges. Therefore, if the group of cut points has high elevation difference along its edges, it will be classified as building points; otherwise, it will be classified as terrain points. For the building points, they will be marked and their elevation in *originalOpen* will be updated with the values from *newOpen*; while for the terrain points, the elevation of *originalOpen* will be unchanged (Figure 1e).

The above procedure will be iteratively performed with progressively increased window sizes until all building points are marked. To find all building areas, the maximum window size should be greater than the size of the largest building, which is denoted as d_{max}. The window size w_i, where $i \in [1, \ldots, n]$, is:

$$w_i = \begin{cases} d_{\min} + 2^i & \text{if } w_i < d_{\max} \\ d_{\max} & \text{if } w_i \le d_{\max} \end{cases}. \quad (5)$$

The illustration of the above procedure is somewhat simplified for clarification. The pseudo code of the actual procedure is as follows:

1. *buildingMask* = 0 # binary image indicating it is a building or not. 1 for buildings and 0 for else
2. *originalOpen* = $\tilde{g}_{o(f\,min)}$
3. for $w_i = w_1$ to w_n
4. *newOpen* = imopen(*originalOpen, w_i*) # open original Open with window size w_i
5. *diff* = *originalOpen-newOpen*
6. create cut areas m_j which satisfy *diff* > 1m
7. remove m_j that are smaller than $d_{min}*d_{min}$ m^2. # the following loop checks whether each binary area m_j is truly a building area or not.
8. for each m_j
9. get the list of *diff* along boundary of m_j, that is, {*diff*($m_{j,b}$)}
10. if min({*diff* ($m_{j,b}$)}) > p_min (condition 1) OR prctile5({*diff* ($m_{j,b}$)}) > p_prctile5 (condition 2) OR prctile20({*diff* ($m_{j,b}$)}) > p_prctile20 (condition 3) OR (prctile80({*diff* ($m_{j,b}$)}) > p_prctile80 AND prctile40 ({*diff* ($m_{j,b}$)}) > p_prctile40) (condition 4), then
11. mark the m_j as a building area
12. end
13. end
14. replace the elevation of *originalOpen* with the value of *newOpen* where those m_j are marked as building areas
15. change the value of *buildingMask* to 1 where those m_j are marked as building areas
16. end

where p_area, p_min, p_prctile5, p_prctile20, p_prctile40, and p_prctile80 are parameters. And, prctile5({*diff* ($m_{j,b}$)}), prctile20 ({*diff* ($m_{j,b}$)}), prctile40({*diff* ($m_{j,b}$)}), and prctile80 ({*diff* ($m_{j,b}$)}) are 5, 20, 40, 80 percentiles of {*diff* ($m_{j,b}$)}, respectively. In code line 9, the boundary cells of m_j are found by subtracting m_i and its morphologically eroded area.

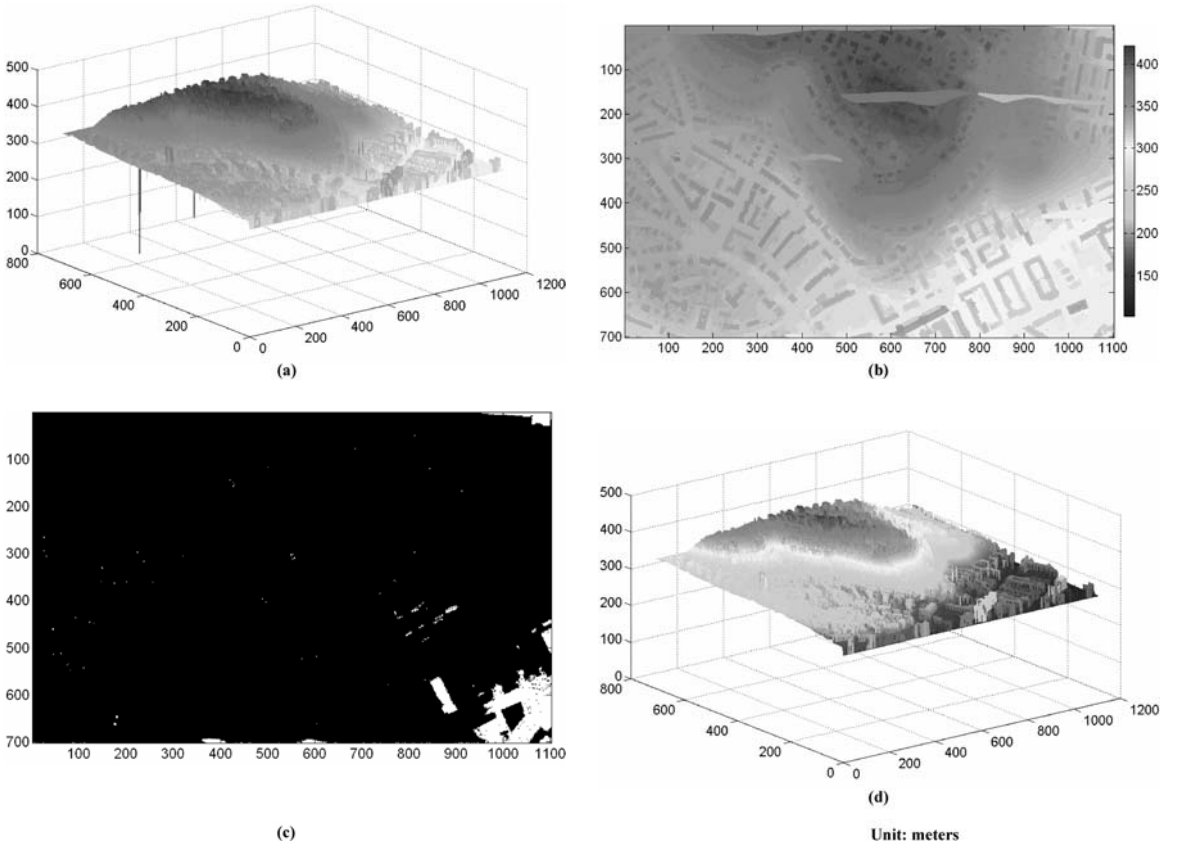

Figure 4. Outlier detection and filling: (a) a 3D view of a grid with outliers, (b) the planer view of this grid, (c) the extended-minima transform of (b) where white stands for the area of regional minima, and (d) the grid after outliers filling. A color version of this figure is available at the ASPRS website: **www.asprs.org.**

The above pseudo code is slightly different from the one-dimensional simplified procedure: first, note that the points in Figure 1 correspond to the cells in a grid and a group of cut points is referred to a cut area here; second, based on the fact that buildings are typically higher than 1 m, only the areas where the differences between *originalOpen* and *newOpen* are greater than 1 m are treated as cut areas (code lines 5 and 6, and see Figure 5a through 5c). Such a setting can reduce the chance of classifying terrain areas as building areas; and third, considering the fact that buildings generally occupy relatively large area, only the areas larger than a certain threshold are chosen to save computation (code line 7). This threshold is set to be $d_{min}*d_{min}$ m^2 because smaller buildings have been removed in $\tilde{g}_{o(f\,min)}$ (Figure 5c).

Another difference is that a combination of conditions, rather than one threshold, is used to determine whether each cut area m_j belongs to buildings or not. The reasons for this are illustrated as follows: originally we assumed that a group of cut points (referred to a cut area in a grid) belongs to either buildings or terrain exclusively (Figure 1d). This assumption is not necessarily true in practice. For example, Figure 5d indicates the cut area for the building X, the major portion of which covers the building while the rest covers the surrounding terrain. This can be easily observed by examining its values of $\{diff(m_{i,b})\}$ for the boundary cells (Figure 6a). The low values $\{diff(m_{i,b})\}$ indicates the positions of terrain covered by m_j. Figure 6b is the histogram of $\{diff(m_{X,b})\}$, where $diff(m_{X,b})$ is list of elevation differences along the boundary of m_X. In such a situation, it is insufficient to differentiate building and terrain cut areas if only based on $\min(\{diff(m_{X,b})\})$ or $\max(\{diff(m_{X,b})\})$. Therefore, the heuristic criteria in code line 10, which characterize the histogram of the $\{diff(m_{X,b})\}$ for a typical building, are used.

There are four conditions for determining whether a cut area m_j is a building or not. In Condition 1, the area is classified as a building if all of its boundary cells are p_min meters higher than the terrain. The value of p_min can be determined by common or prior knowledge of building heights in a study site. In this study, it was set to be 2 m. As indicated in Figure 6b, there are cases where most of the area's boundary cells are 2 m higher than the terrain while some of them are less than 2 m above the terrain. For such cases, it is counted as a building area only if 95 percent of boundary cells are higher than p_prctile5 (Condition 2), or 80 percent of boundary cells are higher than p_prectile20 (Condition 3). Condition 4 is to avoid misclassifying some terrain areas as building areas. Finally, a binary mask for buildings *buildingMask* is created (Figure 5d).

Terrain Returns Identification

A set of terrain pulses is initially identified by calculating the difference between g_{min} and $\tilde{g}_{o(f\,min)}$, excluding the areas indicated by *buildingMask*. Those cells with absolute value of difference less than 0.5 m are treated as terrain. Recall that the X and Y coordinates of the lowest pulse for each cell in g_{min} have been recorded. The triplex $\{X_i, Y_i, g_{min,i}\}$ are extracted to generate a DEM by kriging with the ArcGIS™ 3D Analyst®

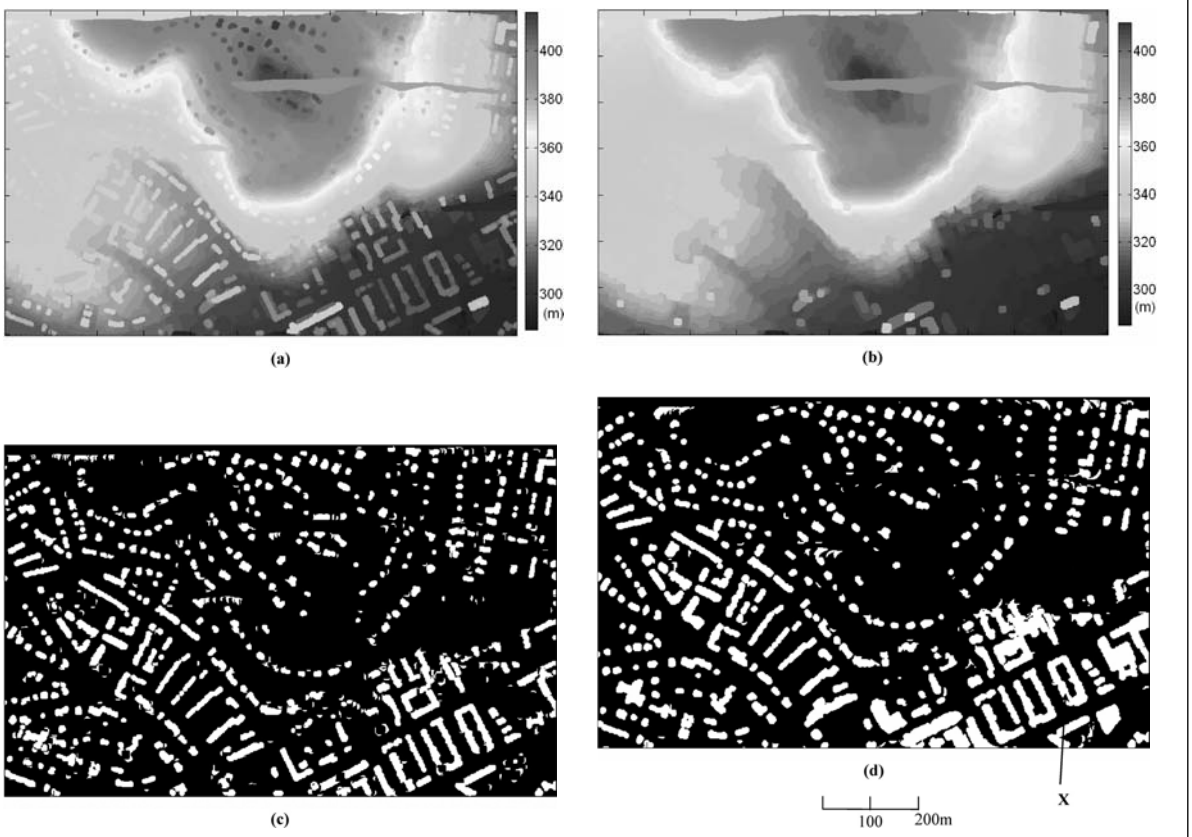

Figure 5. (a) *originalOpen*, (b) *newOpen*, (c) binary grid where each area is larger than d_{min}*d_{min} and *diff* >1 m, and (d) *buildingMask*. A color version of this figure is available at the ASPRS website: **www.asprs.org.**

package. To evaluate the filtering accuracy, a new set of terrain pulses is obtained by comparing the elevation of last return of each pulse with its DEM value. If the absolute value of difference is less than 0.5 m, it is treated as a terrain pulse.

Experiment and Results

Data

The ISPRS Commission III/WG3 dataset includes four urban sites and four rural sites. Since site 8 does not have reference dataset, it was excluded for analysis. For completeness, Table 5.1 on site information in Sithole and Vosselman (2004) is cited as Table 1 here. These sites are located in the Vaihingen/Enz test field and Stuttgart city center, which cover various land-use and land-cover types including buildings, vegetation, river, roads, railroads, bridges, etc. The laser data were collected with an Optech ALTM scanner, with both first and last pulses recorded. The point spacing is 1 to 1.5 m for urban sites and 2 to 3.5 m for rural sites. Moreover, to test the effects of point spacing on filtering, site 1 has data with degraded point density. There are a total of 15 reference samples for testing the filtering accuracy. The reference data were generated by manual filtering with knowledge of the landscape and available aerial imagery (Sithole and Vosselman, 2004).

Parameterization

Table 2 summarizes the parameters used for sites 1 to 7. The parameters d_{min} and d_{max} can be easily determined by trial and error. Recall that d_{min} is the minimal size of structural elements with which vegetation can be removed by morphological opening and d_{max} is the size of the largest building in the site.

For the conditions of differentiating buildings and terrain, their parameters are almost the same for different sites because some characteristics of a building, especially the minimum height, do not vary much even at different places. For example, it is conservative to think that all buildings in an area have a minimum height of 2 m. In this study, all sites except site 5 used the same set of parameters for p_min, p_prctile5, p_prctile20, p_prctile40, and p_prctile80, which were 2 m, 2.5 m, 3 m, 3.5 m, and 5 m, respectively. For site 5, the values for p_prctile20, p_prctile40, and p_prctile80 were 0.5 m smaller than those in other sites because there are some low buildings at this site.

Results

Fifteen reference samples were used to quantitatively assess the accuracy at all sites. The type I, type II, and total errors were calculated for each sample. Due to the limitation of space, only the accuracy table of sample 11 is shown for illustration purpose (Table 3). The type I error is the percentage of bare earth returns misclassified as object returns. The type II error is the percentage of object returns misclassified as bare earth returns. The total error is the error weighted with the portion of each category of reference returns.

The total errors of these fifteen samples for all filtering algorithms reported in Sithole and Vosselman (2004) and our algorithm were summarized in Table 4. Our method obtained the lowest total errors for seven samples. The remaining

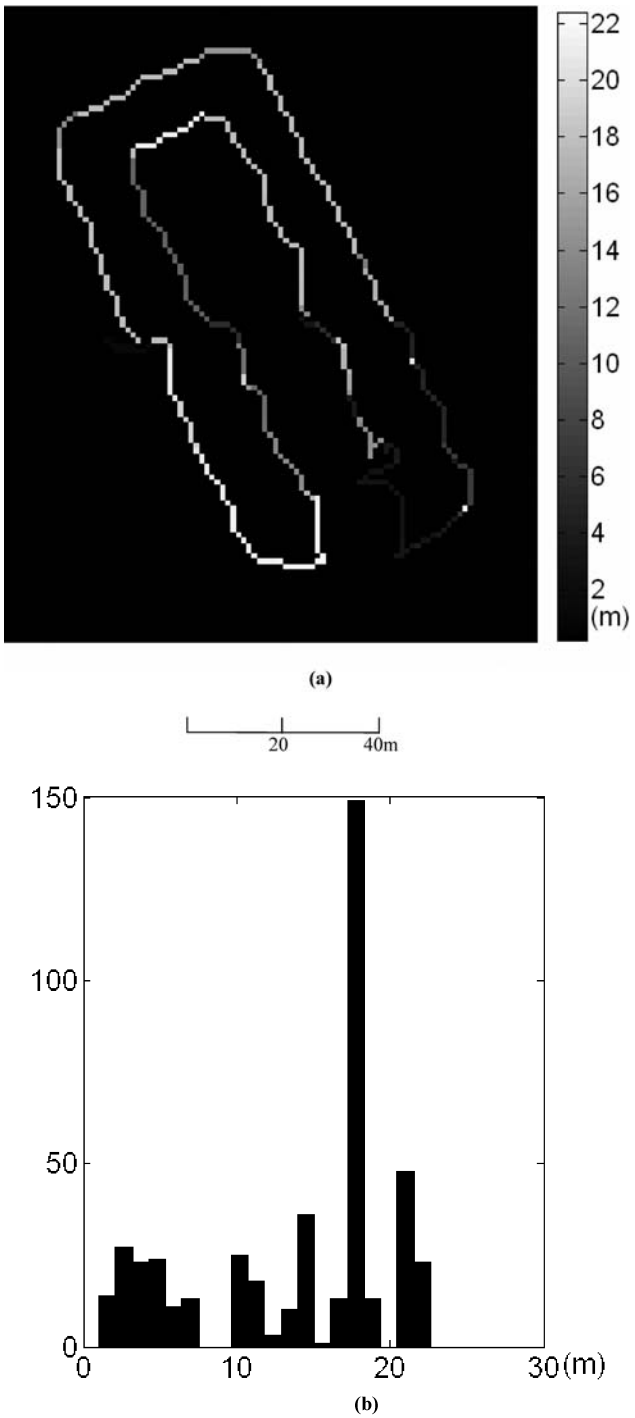

Figure 6. (a) {*diff* ($m_{X,b}$)} along the edge of the building X indicated by X in Figure 5d, and 5b the histogram of {*diff* ($m_{X,b}$)}.

eight samples are close to the lowest errors, except samples 41, 52, 53, and 23. For sample 41, it was found that there are missing data in the north and middle of the area, where is much lower than the terrain after filling. There is also a large group of low outliers and the 100 m^2 threshold cannot remove such a large area of outliers. The abrupt elevation changes caused by both outliers and missing data filling lead to that the terrain was treated as buildings. The total errors for samples 52 and 53 are relatively high (greater than 10 percent). They are both caused by the missing data over the terrain with abrupt changes. The missing data in samples 41, 52, and 53 are all caused by the lack of overlap between swaths. Because the data filling strategy used is to assume that the missing data are caused by water absorption, this problem can be avoided also by a well-planned data collection or changing the ways for filling data. Despite the fact that sample 23 has a total error that is 5.05 percent higher than the lowest error, the results should not be considered too seriously, because it is a complicated scene (Figures 7a through 7c), and it is difficult to define whether some areas belong to bare earth or not (Sithole and Vosselman, 2004).

There are steep slopes in samples 11, 51, and 52. If the effects of missing data are disregarded and then sample 52 is excluded for analysis, it seems that this method can work well over both urban area (sample 11, see Figure 7d through 7f) and forest area (sample 51, see Figure 7g through 7i) with steep slopes. Another advantage of this method is its ability to deal with discontinuity because it is an intrinsic property of morphological opening operation. If building A in Figure 1 was considered as terrain, the opening would not change its shape only if the structural element is smaller than its size.

Effects of Pulse Density

It is important to test the performance of filtering methods in data with different pulse density because lower pulse density implies less cost for acquiring data. Only site 1 was tested since reference data are not available for site 8. The original dataset with point spacing of 1 to 1.5 m was reduced to two new datasets with 2 to 3.5 m and 4 to 6 m point spacing, respectively. The parameters are the same for both original and reduced datasets. Table 5 and Figure 8 show that our algorithm achieved significantly lower total error than other methods for the reduced dataset, even though Axelsson's method is slightly better than our algorithm in the original dataset. Although the test in one site is not sufficient to make conclusive evaluation, the results show this algorithm has encouraging performance in filtering laser scanner data with low pulse density. Note that the same of parameters are used for different point spacing, indicating that not much trial and error is needed for setting parameters.

Discussion

Although the test results demonstrate the ability of this method, it is worthwhile mentioning that the reference data were available after the test results submission deadline for the previous participants. Unlike in this study, they had no chance to optimize their algorithms for these reference samples. Therefore, it is not 100 percent fair to compare this method with those participants.

The focus of this study is the filtering of bare earth and objects (especially vegetation and buildings). However, more research is needed to further differentiate attached (bridges, ramps, etc) and detached (buildings, vegetation, etc) objects (Sithole and Vosselman, 2004). Because these two categories of objects have different patterns of elevation changes around their boundaries, it is possible to extend this method for classifying them. One problem of this method is that it will remove the elevation variations smaller than d_{min} in the opened grid, leading to missed terrain points in over-rugged area. If a very fine DEM at the scale smaller than d_{min} is required, new methods are needed for extracting those terrain pulses.

Conclusions

In this study, a morphological method for filtering laser scanner data is proposed. Such topics as missing data filling, outlier detection, and filtering in urban and vegetated

TABLE 1. DESCRIPTIONS FOR SITE CONDITIONS AND RELEVANT LIDAR DATA

Location	Sites	Special Features	Point Spacing	Samples
Urban	1	Steep slopes, mixture of vegetation and buildings on hillside, buildings on hillside, data gaps	1–1.5 m 2–3.5 m 4–6 m	Sample 11 Sample 12
	2	Large buildings, irregularly shaped buildings, road with bridge and small tunnel, data gaps	1–1.5 m	Sample 21 Sample 22 Sample 23 Sample 24
	3	Densely packed buildings with vegetation between them, building with eccentric roof, open space with mixture of low and high features, data gaps	1–1.5 m	Sample 31
	4	Railway station with trains (low density of terrain points), data gaps	1–1.5 m	Sample 41 Sample 42
Rural	5	Steep slopes with vegetation, quarry, vegetation on river bank, data gaps	2–3.5 m	Sample 51 Sample 52 Sample 53 Sample 54
	6	Large buildings, road with embankment, data gaps	2–3.5 m	Sample 61
	7	Bridge, underpass, road with embankments, data gaps	2–3.5 m	Sample 71

TABLE 2. PARAMETERS USED FOR EACH SITE

Parameters	Site 1	Site 2	Site 3	Site 4	Site 5	Site 6	Site 7
d_{min}(m)	10	10	10	10	10	4	6
d_{max}(m)	42	60	60	50	30	74	42
p_min(m)	2	2	2	2	2	2	2
p_prctile5(m)	2.5	2.5	2.5	2.5	2.5	2.5	2.5
p_prctile20(m)	3	3	3	3	2.5	3	3
p_prctile40(m)	3.5	3.5	3.5	3.5	3	3.5	3.5
p_prctile80(m)	5	5	5	5	4.5	5	5

TABLE 3. ACCURACY ASSESSMENT TABLE FOR SAMPLE 11

Sample 11		Filtered BE	Filtered OBJ	Total	Error
Reference	BE	17607	4179	21786	19.18%
	OBJ	1040	15184	16224	6.85%
	Total	18647	19363	38010	13.92%

area are covered. This method was applied into ISPRS Commission III, WG3 dataset and tested over 15 samples at seven sites. It performed well in many complicated scenes such as areas with discontinuity, large buildings, steep slopes, bridges, ramps, and vegetation on steep slopes. The almost same set of parameters for differentiating buildings and terrain (p_min, p_prctile5, p_prctile20, p_prctile40, and p_prctile80) can be used for different places. When necessary, they only need slight adjustment. Therefore, basically only two parameters (d_{min} and d_{max}) need to be specified in the algorithm, which can be easily determined by trial and error. The major factor affecting the performance is the discontinuity caused by missing data. This situation can be improved with either the advances in sensor design or overlapping swaths of the data.

Acknowledgments

We appreciate the constructive comments from the three anonymous reviewers. Qi Chen is thankful for the support from the NASA Earth System Science Graduate Student

TABLE 4. COMPARISON OF TOTAL ERRORS FOR ALL SAMPLES

Samples	Elmqvist (%)	Sohn (%)	Axelsson (%)	Pfeifer (%)	Brovelli (%)	Roggero (%)	Wack (%)	Sithole (%)	We (%)	Mean (%)	Min (%)	Max (%)
1(Sample11)	22.40	20.49	*10.76*	17.35	36.96	20.80	24.02	23.25	13.92	21.11	10.76	36.96
2(Sample 12)	8.18	8.39	3.25	4.50	16.28	6.61	6.61	10.21	3.61	7.52	3.25	16.28
3(Sample 21)	8.53	8.80	4.25	2.57	9.30	9.84	4.55	7.76	2.28	6.43	2.28	9.84
4(Sample 22)	8.93	7.54	3.63	6.71	22.28	23.78	7.51	20.86	3.61	11.65	3.61	23.78
5(Sample 23)	12.28	9.84	4.00	8.22	27.80	23.20	10.97	22.71	9.05	14.23	4.00	27.80
6(Sample 24)	13.83	13.33	4.42	8.64	36.06	23.25	11.53	25.28	3.61	15.55	3.61	36.06
7(Sample 31)	5.34	6.39	4.78	1.80	12.92	2.14	2.21	3.15	1.27	4.44	1.27	12.92
8(Sample 41)	8.76	11.27	13.91	10.75	17.03	12.21	9.01	23.67	34.03	15.63	8.76	34.03
9(Sample 42)	3.68	1.78	1.62	2.64	6.38	4.30	3.54	3.85	2.20	3.33	1.62	6.38
10(Sample 51)	23.31	9.31	2.72	3.71	22.81	3.01	11.45	7.02	2.24	9.51	2.24	23.31
11(Sample 52)	57.95	12.04	3.07	19.64	45.56	9.78	23.83	27.53	11.52	23.44	3.07	57.95
12(Sample 53)	48.45	20.19	8.91	12.60	52.81	17.29	27.24	37.07	13.09	26.41	8.91	52.81
13(Sample 54)	21.26	5.68	3.23	5.47	23.89	4.96	7.63	6.33	2.91	9.04	2.91	23.89
14(Sample 61)	35.87	2.99	2.08	6.91	21.68	18.99	13.47	21.63	2.01	13.96	2.01	35.87
15(Sample 71)	34.22	2.20	1.63	8.85	34.98	5.11	16.97	21.83	3.04	14.31	1.63	34.98%

Note: The algorithms with the lowest total error are underlined for each sample.

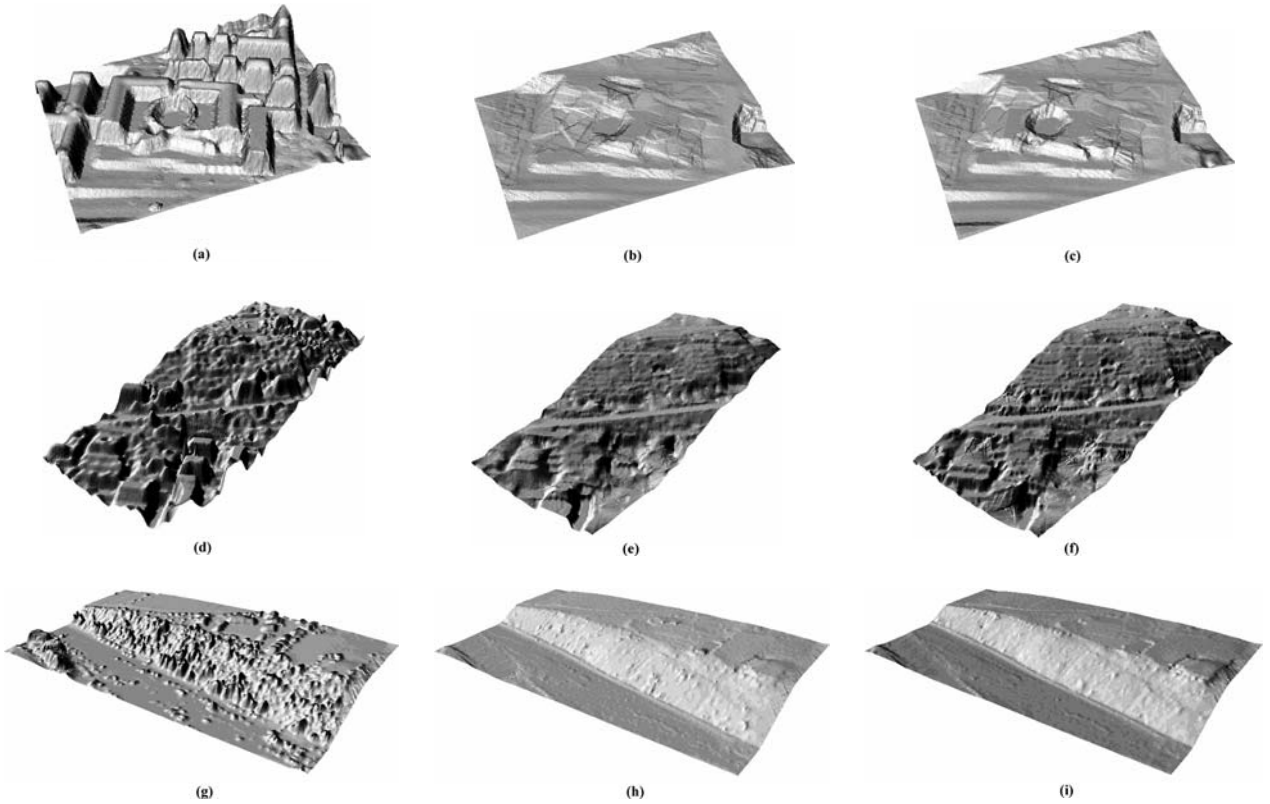

Figure 7. (a) through (c), (d) through (f), (g) through (i) are the DSM, filtered DEM, and true DEM for sample 23, sample 11, and sample 51, respectively.

TABLE 5. COMPARISON OF TOTAL ERRORS IN SITE 1 WITH REDUCED PULSE DENSITY

Samples	Sohn (%)	Axelsson (%)	Pfeifer (%)	Brovelli (%)	Roggero (%)	Wack (%)	Sithole (%)	We (%)	Mean (%)	Min (%)	Max (%)
Sample 11(red1)	30.64	21.11	30.13	40.91	25.42	32.72	29.00	14.64	28.07	14.64	40.91
Sample 11(red2)	38.99	33.34	42.01	40.91	35.06	42.82	37.39	20.89	36.43	20.89	42.82
Sample 12(red1)	15.49	5.47	8.46	22.02	8.13	10.35	9.49	4.49	10.49	4.49	22.02
Sample 12(red2)	18.89	11.17	13.90	NA	12.90	21.10	12.84	7.28	14.01	7.28	21.10

Note: The algorithms with the lowest total error are underlined for each sample.

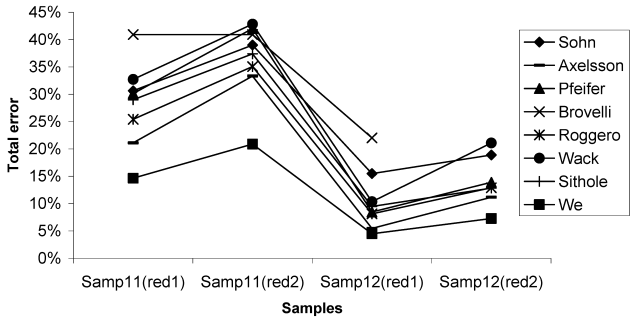

Figure 8. Total errors of different algorithms for the samples with reduced pulse density.

Fellowship and the Berkeley Atmospheric Sciences Center (B.A.S.C) Fellowship.

References

Axelsson, P.E., 1999. Processing of laser scanner data – Algorithms and applications, *ISPRS Journal of Photogrammetry and Remote Sensing*, 54(2–3):138–147.

Axelsson, P.E., 2000. DEM generation from laser scanner data using adaptive TIN models, *International Archives of Photogrammetry and Remote Sensing*, XXXIII (B4), Amsterdam, The Netherlands, pp. 110–117.

Brandtberg, T., T.A. Warner, R.E. Landenberger, and J.B. McGraw, 2003. Detection and analysis of individual leaf-off tree crowns in small footprint, high sampling density lidar data from the eastern deciduous forest in North America, *Remote Sensing of Environment*, 85(3):290–303.

Flood, M., 2001. LIDAR activities and research priorities in the commericial sector, *International Archives of Photogrammetry and Remote Sensing*, XXXIV, WG IV/3, Annapolis, Maryland, pp. 678–684.

Flood, M., and B. Gutelius, 1997. Commercial implications of topographic terrain mapping using scanning airborne laser radar, *Photogrammetric Engineering & Remote Sensing*, 63(4): 327–329, 363–366.

Gong, P., G. Biging, and R. Standiford, 2000. The potential of digital surface model for hardwood rangeland monitoring, *Journal of Range Management*, 53:622–626.

Gong, P., Y. Sheng, and G.S. Biging, 2002. 3D model-based tree measurement from high-resolution aerial imagery, *Photogrammetric Engineering & Remote Sensing*, 68(11):1203–1212.

Haugerud R.A., and D.J. Harding, 2001. Some algorithms for virtual deforestation (VDF) of LIDAR topographic survey data, *International Archives of Photogrammetry and Remote Sensing*, XXXIV, WG IV/3, Annapolis, Maryland, pp. 211–218.

Hoekman, D.H., and C. Varekamp, 1998, High resolution single-pass interferometric radar observation of tropical rain forests trees, *Proceedings of the Second International Workshop on Retrieval of Bio & Geo-Physical Parameters from SAR Data for Land Applications*, 21–23 October, Noordwijk, The Netherlands, European Space Agency, SP 441, pp. 233–240.

Huising E.J., and L.M. Gomes-Pereira, 1998. Errors and accuracy estimates of laser altimetry data acquired by various laser scanning systems for topographic applications, *ISPRS Journal of Photogrammetry and Remote Sensing*, 53(5):245–261.

Kilian, J., N. Haala, and M. Englich, 1996. Capture and evaluation of airborne laser scanner data, *International Archives of Photogrammetry and Remote Sensing*, XXXI (B3), Vienna, Austria, pp. 385–388.

Kraus, K., and N. Pfeifer, 1998. Determination of terrain models in wooded areas with airborne laser scanner data, *ISPRS Journal of Photogrammetry and Remote Sensing*, 53(4):193–203.

Lee, H.S., and N.H. Younan, 2003. DTM extraction of lidar returns via adaptive processing, *IEEE Transactions on Geoscience and Remote Sensing*, 41(9):2063–2069.

Sheng, Y., P. Gong, and G.S. Biging, 2001. Model-based conifer crown surface reconstruction from high-resolution aerial images, *Photogrammetric Engineering & Remote Sensing*, 67(8):957–965.

Sithole, G., and G. Vosselman, 2004. Experimental comparison of filter algorithms for bare earth extraction from airborne laser scanning point clouds, *ISPRS Journal of Photogrammetry and Remote Sensing*, 59(1–2):85–101.

Soille, P., 2003. *Morphological Image Analysis: Principles and Applications*, 2nd Edition, Springer-Verlag, New York, 391 p.

Vosselman G., 2000. Slope based filtering of laser altimetry data, *International Archives of Photogrammetry and Remote Sensing*, XXXIII (B3), Amsterdam, The Netherlands. pp. 935–942.

Zhang, K.Q., S.C. Chen, D. Whitman, M.L. Shyu, J.H. Yan, and C.C. Zhang, 2003. A progressive morphological filter for removing nonground measurements from airborne LIDAR data, *IEEE Transactions on Geoscience and Remote Sensing*, 41(4): 872–882.

(Received 12 July 2005; accepted 03 October 2005; revised 07 November 2005)